



Investigation on the behavior of frozen silty clay subjected to monotonic and cyclic triaxial loading

Xiangtian Xu¹ · Qionglin Li² · Guofang Xu³

Received: 15 November 2018 / Accepted: 30 May 2019 / Published online: 11 June 2019
© Springer-Verlag GmbH Germany, part of Springer Nature 2019

Abstract

This paper aims to assess the characteristics of the deformation and strength behavior of frozen soils at different temperatures under monotonic and cyclic triaxial conditions. The deformation and failure patterns of the specimens change from ductility to brittleness with decreasing temperatures under both monotonic and cyclic loadings. The development of axial strain and stiffness with increasing number of cycles for the soils under cyclic loading is presented and analyzed in detail. A collapse behavior in strength and stiffness is observed in tests of frozen soils at $-5\text{ }^{\circ}\text{C}$, $-7\text{ }^{\circ}\text{C}$ and $-9\text{ }^{\circ}\text{C}$. The difference in frictional sliding between the samples with high ductility and those with high brittleness is attributed to the different patterns of deformation and failure. The dynamic modulus is plotted versus axial strain, and the state where the stiffness begins to decrease is employed as the criterion of cyclic failure. The proposed criterion of cyclic failure is verified to be more suitable for frozen soils with high brittleness and seems to be consistent with the peak strength under monotonic loading. Finally, the cyclic stress ratios are plotted against the number of cycles up to this failure criterion, and the effect of temperatures on cyclic strength is evaluated.

Keywords Cyclic strength · Deformation mechanism · Frozen soils · Stiffness · Triaxial test

1 Introduction

In recent years, an increasing number of construction projects are being carried out throughout the cold regions of the world, and the effective design of foundations for stable structures in cold regions requires detailed knowledge of the strength and deformation characteristics of frozen soil and the influence of temperature on its behavior [6, 21, 25, 26]. In addition, the technique of artificial ground freezing is often used as a construction aid to

control groundwater or provide temporary support for excavations, tunnels and mineshafts [9, 10, 13, 33]. However, the greater use of such a construction aid is limited due to the lack of detailed understanding and accurate modeling of the behavior of frozen soils under different loading and temperature conditions. Therefore, there is an ongoing demand for the study of the mechanical behavior of frozen soils and the effect of temperature on that behavior.

Understanding and predicting the mechanical behavior of frozen soils is a difficult problem because of the presence of ice and unfrozen water, the complex microscopic mechanisms controlling the strength of the soil and the sensibility of the soil to temperature [3, 15, 20, 27]. Extensive investigations have been conducted on the mechanical behavior by many researchers for more than 50 years, focusing on the deformation and failure processes under monotonic and cyclic loadings, and the triaxial test apparatus has found widespread application in such investigations [4, 8, 12, 15, 20, 22–24, 29, 34, 38]. These studies reveal that the deformation of frozen soils is highly nonlinear under both types of loadings [2, 8, 16, 32, 34, 37, 39]. The stress–

✉ Qionglin Li
qionglin_li@126.com

¹ Institute of Transportation, Inner Mongolia University, Hohhot 010070, People's Republic of China

² Key Laboratory of Earthquake Engineering and Engineering Vibration, Institute of Engineering Mechanics, China Earthquake Administration, Harbin 150080, People's Republic of China

³ State Key Laboratory of Geomechanics and Geotechnical Engineering, Institute of Rock and Soil Mechanics, Chinese Academy of Sciences, Wuhan 430071, People's Republic of China

strain response under monotonic loading is usually used to determine the initial yield stress, the strength and small-strain stiffness [2, 8, 20, 28, 29], while the accumulated deformation and stiffness changes within the increasing number of loading cycles under cyclic loading are often used to understand the dynamic behavior of frozen soils [17, 18, 34, 36]. Furthermore, the effect of frozen temperature, confining pressure, cyclic stress amplitude and some other critical factors on the monotonic or cyclic behavior of different frozen soils have been investigated in these studies. Based on a literature review, the following conclusions can be made: (i) A soil will achieve high strength and stiffness during the freezing process and both of the above parameters increases with decreasing temperature. The ice lens and the cementation in the solid soil matrix are often attributed to the increase in strength and stiffness [20, 35]. As the temperature decreases from 0 °C, the thickness of the strongly bonded unfrozen water layer around grains decreases, and hence, the cementation in the soil matrix increases. Furthermore, the content of ice lenses in the void between the soil matrices increases, which will enhance the hindrance of the soil grain deformation during loading. (ii) The effect of confining pressure on the strength is drastically different for a soil in frozen and unfrozen states. The strength of frozen soils increases gradually in the low confining pressure stage and then decreases with increasing confining pressure [5, 24, 28]. The pressure melting under high confining pressure is attributed to such changes with the confining pressure. (iii) Published cyclic test data show that the accumulation mode of plastic strain of frozen soils is found to be depended on the applied cyclic stress amplitude [17, 18, 34, 36]. The accumulated strain of frozen soils increases and then tends to level off with the number of cycles under low-amplitude cyclic stress, while the plastic strain accumulates with an increasing rate and rapidly reaches the failure limit of the frozen soils under high-amplitude cyclic stress. (vi) The frozen soil stiffness changes remarkably with the number of loading cycles; recent studies, including Ling et al. [19], Li et al. [17], Liu et al [18], have conducted cyclic triaxial tests to capture the stiffness changes with increasing loading cycles, and the change modes were found to be depended on the cyclic stress amplitude.

Although much work has been done, a qualitative understanding of basic frozen soil behavior is still, for the most part, lacking in the literature, and the details are summarized as follows: (i) In the previous studies, the monotonic and cyclic behaviors of frozen soils have been usually investigated separately; however, the connections between them are rarely studied to date. The differences and similarities between the deformation mechanisms of frozen soils under monotonic and cyclic loading need be investigated, which will be useful to develop a united

constitutive model that describes both monotonic as well as cyclic behaviors uniformly; (ii) Attempts have been made in the recent years to tackle this issue of stiffness changes in frozen soils under cyclic loading, and the dependence of stiffness changes in deformation history has been found in our recent studies [17, 19]; however, not enough results can be used to understand the dependence between them and further investigations need be conducted. (iii) Although the issue of the strength behavior of frozen soils has been addressed extensively for monotonic loading conditions, there is no reasonable metrics used to quantify strength under cyclic loading [1, 12, 17, 18, 27], which prevent us to estimate the stability of foundations or geo-structures in cold regions subjected to cyclic loading, such as occurs during the vibration of machinery, drilling equipment or seismic activity in cold regions. (vi) Most of the existing triaxial tests for frozen soils were conducted under high confining pressure to investigate the effect of pressure melting, which is not suitable for most routine geotechnical problems such as building foundations in cold regions. Knowledge of the strength and deformation behavior of frozen soils under medium and low confining pressure is still required to design and carry out such construction projects in cold regions.

Recognizing the necessity to adequately capture further behaviors of frozen soils as described above, this study extends this research topic by conducting the monotonic and cyclic triaxial tests under the identical confining pressure of 200 kPa, which is common in most routine geotechnical problems. The changes in the stress–strain derived from monotonic tests are presented, and the effect of temperature on the deformation model, strength and stiffness are analyzed first in light of the response observed from samples with identical origins in an unfrozen state. Next, the typical stress–strain response under cyclic loading is also presented and investigated in detail. Subsequently, the changes in axial strain and stiffness versus number of loading cycles are studied and the dependence of stiffness changes on the deformation history are analyzed and interpreted by the same deformation mechanism of frozen soils under monotonic loading. Based on the results of stiffness changes, the criterion of cyclic strength is finally proposed for the frozen soils with high brittleness, and then, this criterion is verified to be consistent with the peak strength under monotonic loading.

2 Experimental program

2.1 Material and specimen preparation

A soil from the Qinghai-Tibet Plateau (near the Beilu River, along the Qinghai-Tibet railway) was used in this

experimental investigation. Prior to testing, the soil was air-dried for 2 weeks and passed through a sieve with an aperture size of 2.0 mm. This soil is classified as silty clay according to the Chinese Soil Classification System, and the specific gravity of the solids is 2.64. According to standard procedures (GB/T50123-1999), the basic index properties of this soil (after removal of material > 2.00 mm) were determined and are summarized as follows. The liquid limit of this soil is 28%, the plasticity limit is 17.7%, and the plasticity index is 10.3. Standard compaction tests were conducted to determine the maximum dry density and the optimum moisture content, which were 1.828 g/cm^3 and 14.8%, respectively. The grain size distribution of this soil is shown in Fig. 1.

The reconstituted artificial frozen soil specimens were prepared in the laboratory. The specimens had a diameter of 50 mm and a height of 100 mm, and the procedures performed as follows. The desired water content (e.g., 15%) was added to the dry soil and mixed uniformly. A steel split mold with an inside diameter of 50 mm and a height of 100 mm was used to prepare the specimens. Each sample was compacted through three layers according to the standard procedure (GB/T50123-1999) and then removed from the steel mold. A cylindrical specimen with the desired size was produced with a bulk density of 1.96 g/cm^3 and was used in the tests under unfrozen conditions. However, more procedures are needed to produce the frozen samples. To avoid large frost heaving and significant moisture movement during freezing, each specimen was then mounted in a steel split mold, which was specifically manufactured and fixed at two ends by a steel frame. Subsequently, the specimen was placed in a freezer at a temperature of $-30 \text{ }^\circ\text{C}$ for 12 h to freeze rapidly.

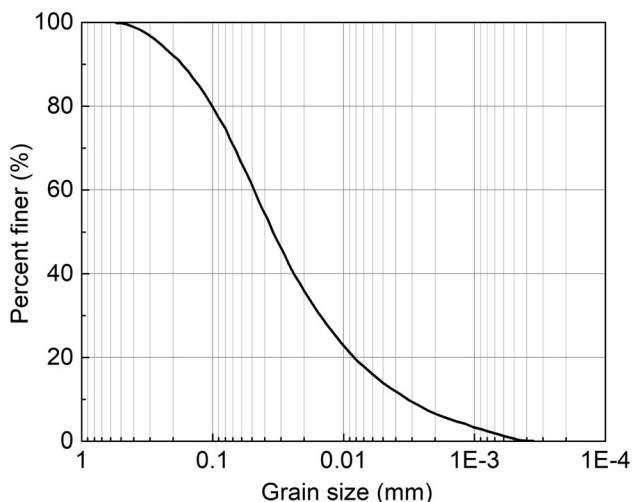


Fig. 1 Particle size distribution of the tested silty clay

2.2 Test device and testing procedure

In the present study, both the monotonic and cyclic triaxial tests were performed using a computer-controlled GDS triaxial testing system. The main system components comprise the following items: signal conditioning, a servo amplifier, a computer interface and data acquisition units. The vertical loading system consists of a load frame and an axial actuator, and this apparatus is capable of carrying out stress- or strain-controlled loading. This configuration can apply axial stress or strain loading with a maximum frequency of 10 Hz using built-in sine, triangular, and square waveforms or any other random waveforms defined by means of external input. A new triaxial cell equipped with a temperature control system was developed. Three U-shaped copper tubes were placed in the triaxial cell and connected to a cold bath. The triaxial cell was insulated with a polyether high density hard layer, and temperature sensors were installed to measure the liquid temperature in the triaxial cell. Simethicone is selected to apply cell pressure through servo valves and used as the cooling medium in a refrigeration system. The temperature control system can set the liquid temperature in triaxial cells in the range of $\pm 0.1 \text{ }^\circ\text{C}$ around the determined value. The maximum cell pressure, the maximum axial force, the maximum axial displacement and the lowest temperature in the triaxial cell are 20 MPa, 200 kN, 60 cm and $-30 \text{ }^\circ\text{C}$, respectively.

A prepared specimen was taken from the storage freezer ($-30 \text{ }^\circ\text{C}$) prior to testing, removed from the split mold, covered with a rubber membrane and then placed between filter papers, steel plates and the top and bottom load platens. Four to six O-rings were used to provide a water-tight seal between the membrane and the load platens, and then, the triaxial cell was filled with simethicone. Subsequently, the temperature control system was used to get the liquid in the triaxial cell to the selected temperature for the triaxial test. This procedural step lasted for 12 h to stabilize the cell liquid temperature at the desired test temperature and ensure that the temperature in the specimen was uniform throughout.

In the monotonic triaxial test, each sample was first subjected to a determined isotropic confining pressure of 200 kPa for 10 min, and then, a constant axial deformation rate was applied to the specimen, while the radial stress was kept constant during the entire test. For this test type, loading was suspended until vertical deformation had reached the determined limit of 15 cm. As shown in Fig. 2(a), the loading process of the cyclic triaxial test consisted of five sequences. The cell pressure was first applied to the liquid in the cell to create an isotropic stress around the specimen, and this step lasted for 0 min.

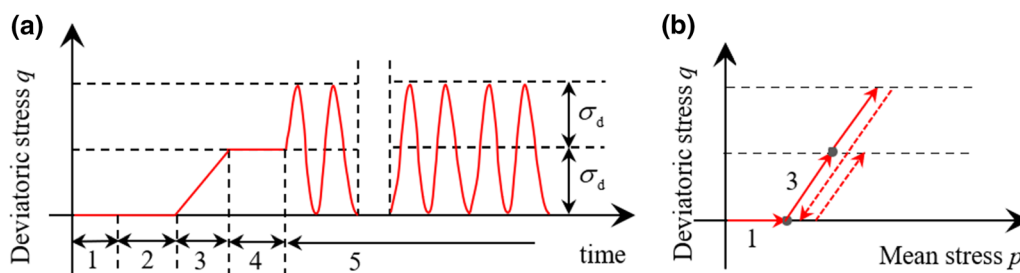


Fig. 2 Schematic illustration of **a** applied loading sequence on specimen; **b** typical stress path in cyclic tests

Subsequently, the applied axial stress on the sample was increased to a value equal to the desired amplitude of cyclic stress, σ_d , with a constant rate of axial force of 0.2 kN/s. The specimen was kept for 30 s under this stress state to stabilize the applied stress, and then, one-way cyclic loading without stress reversal, expressed as additional force to the initial axial stress, was imposed in the axial direction. The loading pattern was a sine wave, as shown in Fig. 2a. In each test, cyclic stress with identical amplitude was applied to the specimen in a stress-controlled mode and at a frequency of 1.0 Hz. Changes in the axial deformation and axial stress were measured during cyclic loading. The cyclic loading was suspended after 1000 cycles or until axial strain had reached the determined limit. For the soils in an unfrozen state, the limit is 20%, while that of the soils in a frozen state is 10%. The details of each test are listed in Table 1.

In accordance with the sign convention in soil mechanics, compressive stress and contraction are defined as positive, whereas tensile stress and elongation are defined as negative. The general stress invariants are described using “Cambridge $p-q$ ” stress parameters, where deviatoric stress is defined as ($q = \sigma_1 - \sigma_3$), and mean stress as $p = (\sigma_1 + 2\sigma_3)/3$, with σ_1 and σ_3 being the major and minor principal stresses. A schematic of the typical stress path is also presented in Fig. 2b, and the cyclic stress path in each test is identical.

3 Experimental results and discussion

3.1 Monotonic triaxial test

As shown in Table 1, four monotonic triaxial tests under undrained conditions were carried out at temperatures between $-3\text{ }^\circ\text{C}$ and $-9\text{ }^\circ\text{C}$. In addition, another triaxial test was performed on a sample in an unfrozen state to investigate the effect of freezing temperature on the stress–strain response. The deviatoric stress–axial strain curves derived from all the monotonic tests are shown in Fig. 3. Typically, deviatoric stress increases linearly at the very beginning of each test, which could be attributed to elastic

response, followed by yielding (peak strength). However, different post-peak stress–strain responses are exhibited for the tests in different frozen states. Each deviatoric stress–axial strain response derived from tests Nos. 1 and 2 exhibits a rounded peak value, followed by the deviatoric stresses decreasing smoothly with increasing axial strain until reaching an approximately constant value (residual strength). The results of tests Nos. 3, 4 and 5 show more brittle responses, in which the deviatoric stress decreases rapidly after a sharp peak and the approximate residual strengths are usually reached at large axial strain. The differences in the post-peak stress–strain response indicate that more brittle behavior is induced by the lower temperature.

The peak deviatoric stress and the secant modulus at the axial strain level of 1% obtained from every test are selected to investigate the effect of freezing temperature. As shown in Fig. 3, the deviatoric stress increases linearly before the axial strain reaches 1%; therefore, $E_{0.01}$ could be attributed to the elastic modulus. To evaluate the effect of freezing temperature on the strength and stiffness of frozen soils, the values of soils in an unfrozen state are selected as references, and the strengthening factors are defined as

$$\lambda_p = q_{\text{peak}}/q_{\text{peak,ref}} \quad (1)$$

$$\lambda_E = E_{0.01}/E_{0.01,ref} \quad (2)$$

where λ_p and λ_E are the strengthening factors of the peak strength and stiffness, respectively, $q_{\text{peak,ref}}$ is the reference value of the peak strength and $E_{0.01,ref}$ is the reference value of the elastic modulus. As described before, the reference values of the peak strength and elastic modulus are obtained from the specimen in an unfrozen state. The strengthening factors of the peak strength and stiffness are plotted in Fig. 4 as a function of temperature. It is clearly shown that a decrease in the temperature results in the mobilization of high peak strength and stiffness, as expected from past studies [7, 14, 32]. Furthermore, λ_p and λ_E approach the same value at each temperature, and the temperature dependency of both of these variables can be expressed by a linear regression equation as follows:

$$\lambda_p \text{ (or } \lambda_E) = a + bT \quad (3)$$

Table 1 Details of monotonic and cyclic triaxial tests

Test group	Test no.	σ_3 (kPa)	Strain rate ($10^{-5} s^{-1}$)	σ_d (kPa)	Temperature ($^{\circ}C$)
Group A: monotonic loading	1	200	1.67	–	Room temperature
	2	200	1.67	–	– 3
	3	200	1.67	–	– 5
	4	200	1.67	–	– 7
	5	200	1.67	–	– 9
Group B: cyclic loading	6	200	–	400	Room temperature
	7	200	–	500	Room temperature
	8	200	–	600	Room temperature
	9	200	–	800	– 3
	10	200	–	900	– 3
	11	200	–	1000	– 3
	12	200	–	1100	– 3
	13	200	–	900	– 5
	14	200	–	1000	– 5
	15	200	–	1100	– 5
	16	200	–	900	– 7
	17	200	–	1200	– 7
	18	200	–	1350	– 7
	19	200	–	1450	– 7
	20	200	–	900	– 9
	21	200	–	1500	– 9
	22	200	–	1800	– 9

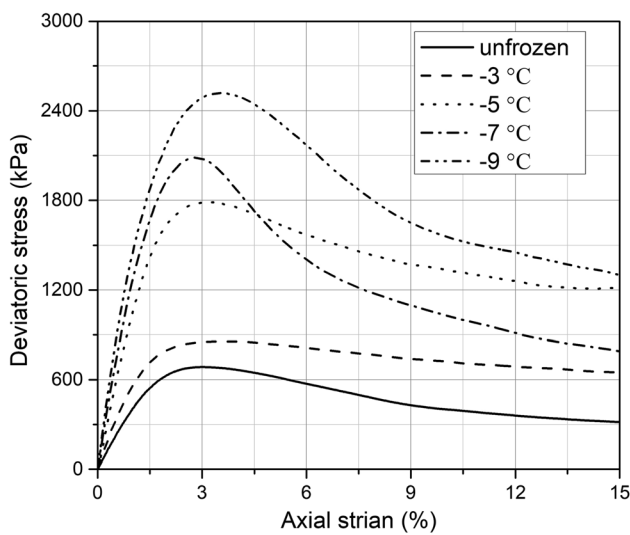


Fig. 3 Deviatoric stress-axial strain curves for the specimens under different temperatures

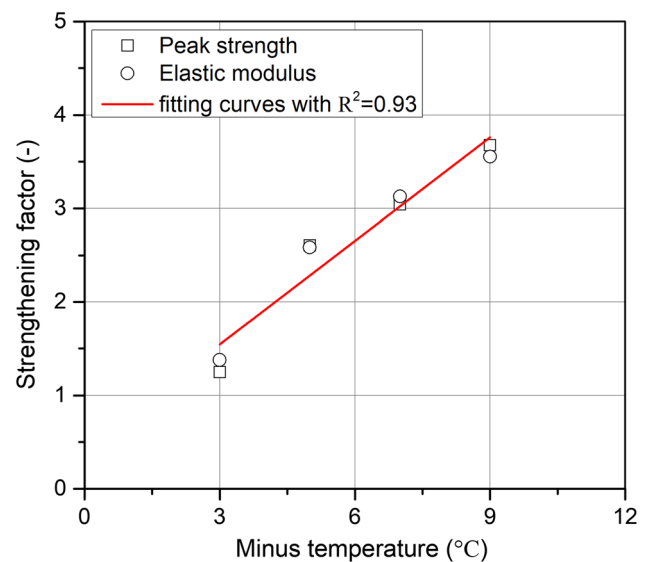


Fig. 4 Strengthening factors of peak strength and stiffness versus minus temperature

where a is the intercept, b is the coefficient ($/^{\circ}C$) and T is the minus temperature ($^{\circ}C$). The best-fit linear regression equation derived from using to the data and the resulting coefficient of correlation are shown in Fig. 4. The high coefficient of correlation ($R^2 = 0.93$) means that the effect

of temperature on the peak strength and stiffness can be described well in the range of test temperature.

The temperature dependency of the strength and stiffness behavior can be attributed to two possible reasons: the

ice lens and the cementation in the solid soil matrix. With a decrease in temperature, the ice content of frozen soils increases, and the cementation between the intergranular interfaces becomes strong; hence, the sliding and rearrangement of the soil particle skeleton will be restricted during loading.

3.2 Cyclic triaxial test

Only the deviatoric stress-axial strain curves of frozen samples at $-5\text{ }^{\circ}\text{C}$ are selected and plotted in Fig. 5 for the purpose of brevity. Corresponding with the loading sequences shown in Fig. 2a, the development of axial strain was clearly divided into three sequences. In the first loading sequence, the axial strain increases until the deviatoric stress reaches the determined level. Thereafter, the deviatoric stress remains constant; however, the axial strain also increases for 30 s, which could be attributed to the

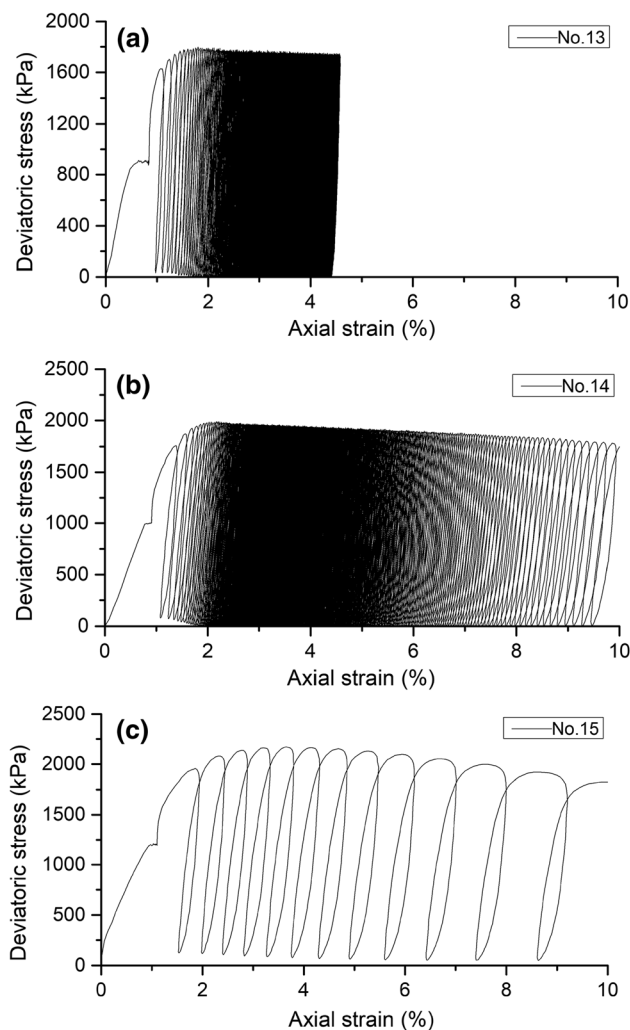


Fig. 5 Cyclic deviatoric stress-axial strain curves for frozen the specimens under $-5\text{ }^{\circ}\text{C}$

strong creep behavior of frozen soils. In the cyclic loading sequence, the stress–strain curve shows hysteresis and accumulation of irreversible strains with increasing number of cycles. The characteristic features of the hysteresis loops and some conclusions drawn from the curves in Fig. 5 are as follows: (i) No closed hysteresis loop is induced by each loading cycle, which means that frozen samples exhibit significant elastoplastic behavior during cyclic loading and that the imposed cyclic stress lies outside the true elastic range even for test No. 13. (ii) During the cyclic loading, the plastic or irreversible strains become large with the increasing number of loading cycles, and the higher cyclic loading results in more residual strain after the same number of loading cycles. (iii) The differences in residual axial strain between two adjacent cycles show different changes for the samples under different cyclic stress levels. For test No. 13, the differences decrease during the whole loading cycles; however, the results of tests Nos. 14 and 15 show that the differences decrease in the initial loading cycles and then increase with successive loading cycles. The changes are different from the conclusions drawn by Liu et al. [18], in which only decreases in the differences were found. The low confining stresses (lower than that applied in the studies of [18]) in our studies may contribute to this special phenomenon. It is clearly shown that the frozen soils exhibit more brittle behavior under lower confining stress.

The characteristic features of the hysteresis loops will be further examined by comparing the evolution of deformation and stiffness against the number of loading cycles. For this purpose, the typical deviatoric stress-axial strain is schematically depicted in Fig. 6. In the discussion that follows, the loading cycles are reintegrated, and one cycle includes one loading and one unloading process. It is clear that the loop O-A-B-C-D is a nominal cycle because it covers the initial loading stage and creep loading stage; hence, this loop will not be used in the following study.

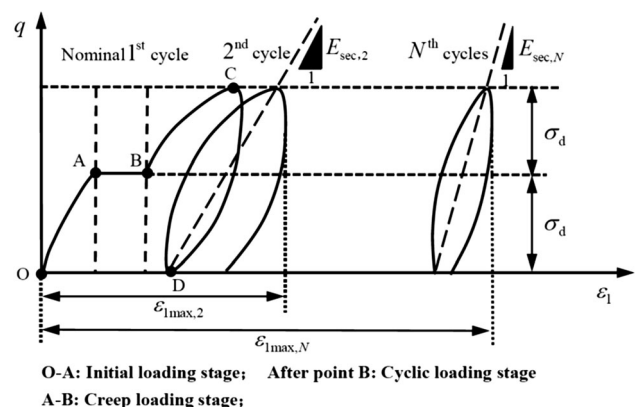


Fig. 6 Schematic illustration of cyclic deviatoric stress-axial strain curves

The dynamic modulus, $E_{sec,N}$, is the secant stiffness calculated from the strains induced by the loading process in the N th cycle. $\varepsilon_{a,N}$ indicates the maximum axial strain at the N th cycles. It should be noted that the maximum axial strain usually does not correspond to the peak point of the hysteresis loop and occurs in the unloading process of each cycle, which also indicates the significant creep behavior of frozen soils.

The evolution of the dynamic modulus and maximum axial strain with increasing loading cycles are presented in Figs. 6, 7, 8, 9 and 10. The test results of Nos. 6, 7, 9, 10 and 11 show similar development patterns of the dynamic modulus and axial strain with increasing loading cycles. The dynamic modulus, E_{sec} , increases rapidly to a peak value in the initial few loading cycles and then decreases smoothly. It can be observed that the inflection point (shown by a gray dot in the figures) divides the development of $\varepsilon_{a,N}$ into two stages in the curve of $\varepsilon_{a,N} - N$. The maximum axial strain, $\varepsilon_{a,N}$, increases rapidly in stage 1, which is followed by an approximately linear growth in the subsequent stage. In addition, the peak point of the dynamic modulus corresponds to the inflection point of the maximum axial strain, which means that the initial increase and the subsequent decrease of the stiffness correspond to stages 1 and 2, respectively. Test No. 8 exhibits a special behavior, as shown in Fig. 7c. The stiffness increases smoothly in the initial few cycles and remains at an approximate constant value, while the maximum axial

strain growth shows strong linearity, and no marked inflection point is observed during the whole loading process.

For the frozen samples at relatively low temperatures, such as tests Nos. 13, 16 and 20, the development of both dynamic modulus and maximum axial strain with increasing loading cycles exhibits similar evolution patterns. It can be seen from the results derived from these tests that the change in E_{sec} and $\varepsilon_{a,N}$ induced by the initial loading cycles is greater than the change for subsequent cycles.

The patterns of the evolution of E_{sec} and $\varepsilon_{a,N}$ for tests Nos. 14, 15, 17, 18, 21 and 22 are qualitatively similar. The stiffness and deformation of these specimens experience three stages from the beginning of the loading till the final axial strain of 10%. It can be observed that E_{sec} and $\varepsilon_{a,N}$ rapidly increase to the first marked yield point in stage 1 with a decreasing rate. In stage 2, the dynamic modulus, E_{sec} , seems to vary around a constant value or decreases smoothly, while the maximum axial strain, $\varepsilon_{a,N}$, increases with an approximate linear pattern. The response in this stage means that the complete breakdown of the frozen soils does not take place immediately after the first primary yield. The behavior in the initial two stages is qualitatively similar to the behavior observed in the samples labeled with Nos. 6, 7, 9, 10 and 11. However, for the samples of Nos. 14, 15, 17, 18, 21 and 22, there is another marked yield point, which separates the plateau of smoothly

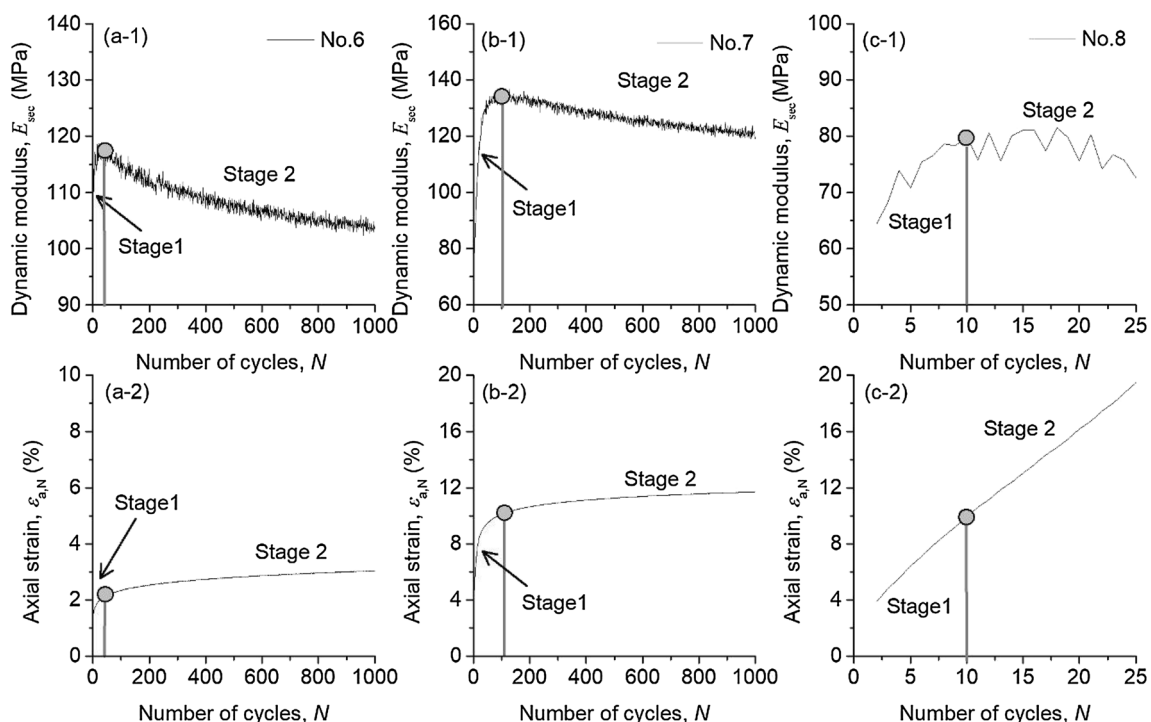


Fig. 7 Characteristics of dynamic modulus and maximum axial strain of soils under unfrozen state during cyclic loading **a** test No. 6 ($\sigma_d = 400$ kPa); **b** test No. 7 ($\sigma_d = 500$ kPa); **c** test No. 8 ($\sigma_d = 600$ kPa)

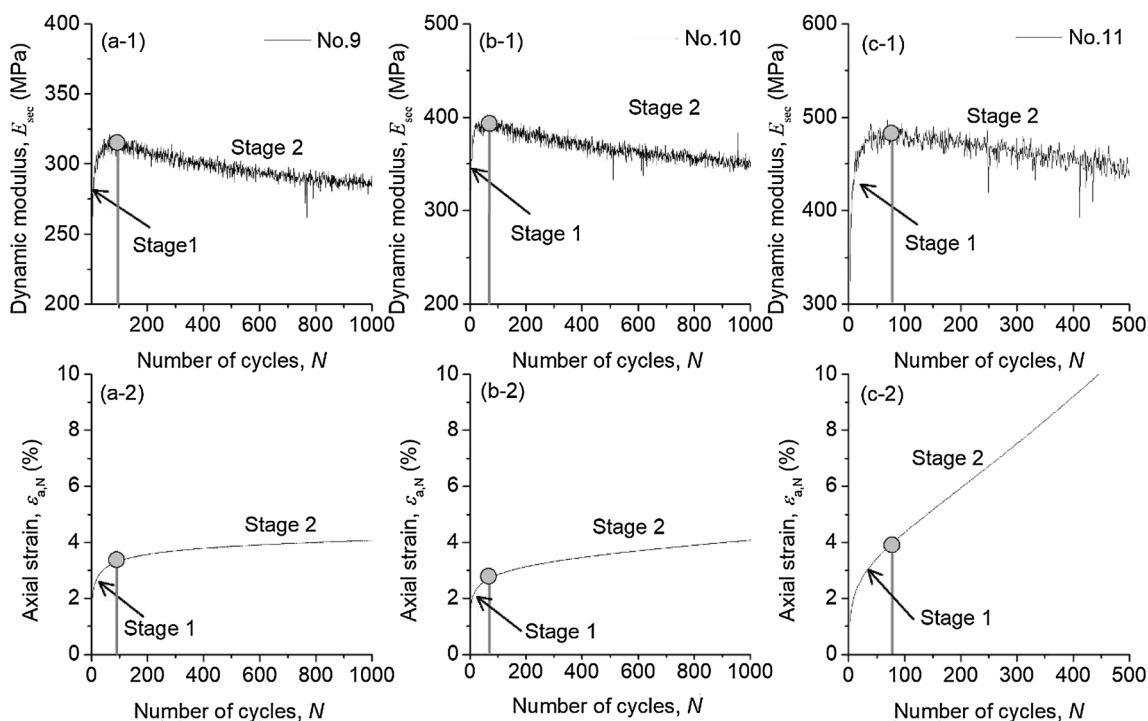


Fig. 8 Characteristics of dynamic modulus and maximum axial strain of soils under -3°C during cyclic loading **a** test No. 9 ($\sigma_d = 800\text{ kPa}$); **b** test No. 10 ($\sigma_d = 900\text{ kPa}$); **c** test No. 11 ($\sigma_d = 1000\text{ kPa}$)

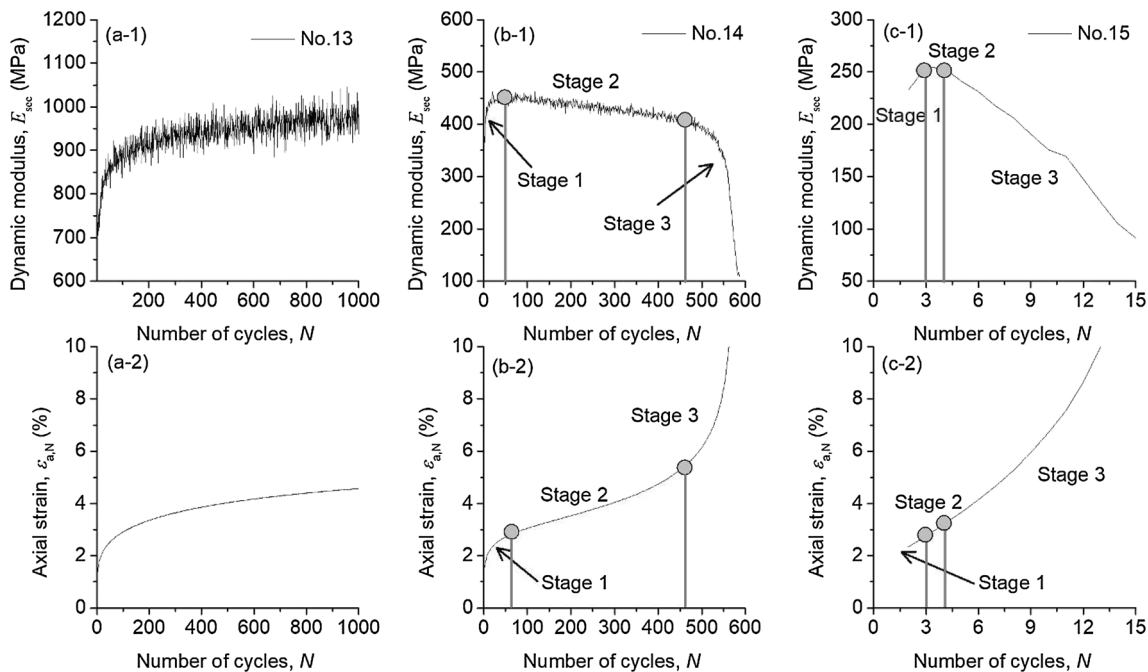


Fig. 9 Characteristics of dynamic modulus and maximum axial strain of soils under -5°C during cyclic loading **a** test No. 13 ($\sigma_d = 900\text{ kPa}$); **b** test No. 14 ($\sigma_d = 1000\text{ kPa}$); **c** test No. 15 ($\sigma_d = 1100\text{ kPa}$)

changing stiffness from the start of substantial stiffness degradation. In the last stage, the collapse responses with a

rapid reduction in E_{sec} and an accelerated increase in $\epsilon_{a,N}$ are observed with successive loading cycles.

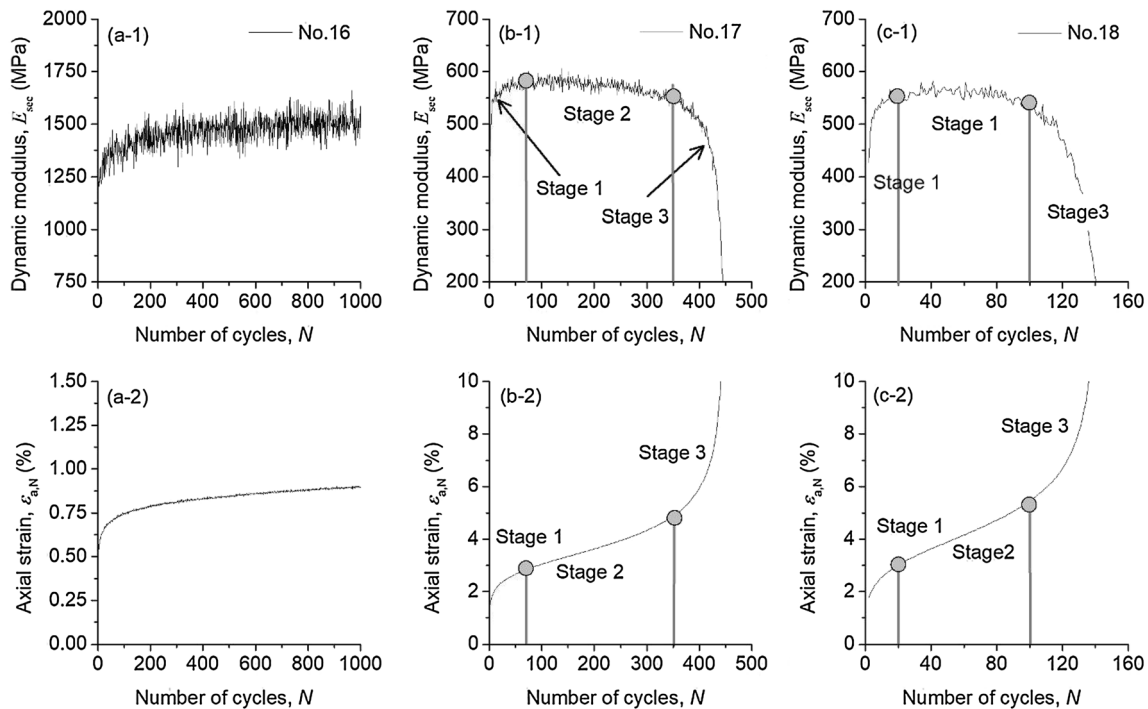


Fig. 10 Characteristics of dynamic modulus and maximum axial strain of soils under -7°C during cyclic loading **a** test No. 16 ($\sigma_d = 900$ kPa); **b** test No. 17 ($\sigma_d = 1200$ kPa); **c** test No. 18 ($\sigma_d = 1350$ kPa)

Furthermore, it can also be observed that the samples subjected to relatively high cyclic stress (tests Nos. 8, 11, 14, 15, 17, 18, 21 and 22) reach the test limit in fewer than 1000 loading cycles. As described before, the samples in the unfrozen state (test No. 8) and -3°C (test No. 11) exhibit an approximately linear increase in $\varepsilon_{a,N}$ and a nearly constant or smooth decrease in E_{sec} , while the samples below -3°C (tests Nos. 14, 15, 17, 18, 21 and 22) show large losses in stiffness and accelerated axial deformation during loading near the end cycles. The different responses indicate that the samples in the unfrozen state and at -3°C exhibit significant ductility, while the samples below -3°C show brittle behavior. This finding is consistent with the conclusions derived from the monotonic triaxial tests conducted in this study. Based on the above conclusions, it is believed that the freezing temperature of soils will change the deformation patterns under both monotonic as well as cyclic loadings and that the lower temperature is linked with more brittle behavior.

The axial deformation of unsaturated soils under triaxial compression conditions is often derived from several mechanisms, such as volume compaction and frictional sliding. In the initial loading stage, the axial deformations are mainly derived from the volume compaction of the samples, and the successive strain hardening results in a progressive decrease in the deformation rate and an increase in stiffness. In the subsequent loading stages, the frictional sliding of the shear band in the samples mainly

induces growth of the axial deformation. The differences in the deformation patterns for the samples at different temperatures are mainly exhibited in the range of frictional sliding, as presented in Figs. 7, 8, 9, 10 and 11. For the samples in an unfrozen state or at a relatively higher frozen temperature (referred to as -3°C in this study), the cementation between soil particles is weak, and the shear deformation in the thickness direction of the shear band is continuous, which results in an approximately linear increase in axial strain to a large value. Furthermore, compared with the rapid increase in stiffness in the initial stage, the change in stiffness is small and tends to level off with subsequent loading cycles. This observation means that the deformation of the test samples approached the critical state as expected, which has been verified by many results from tests conducted previously [30, 31]. Meanwhile, the bond in frozen soils at low temperature (referred to as the samples at -5°C , -7°C and -9°C in this study) is strong enough, and the frictional sliding process is similar to the fracturing of solid materials. At the beginning of frictional sliding, the stress concentrations that occur around the solid particles result in tiny cracks between the grains and the ice matrix that propagate from particle to particle in the shear bond. In the process of crack propagation, the shear zone grows continually; however, the changes in frictional resistance of the overall sample are small. This corresponds to the approximately linear increase in axial strain and the plateau of smoothly

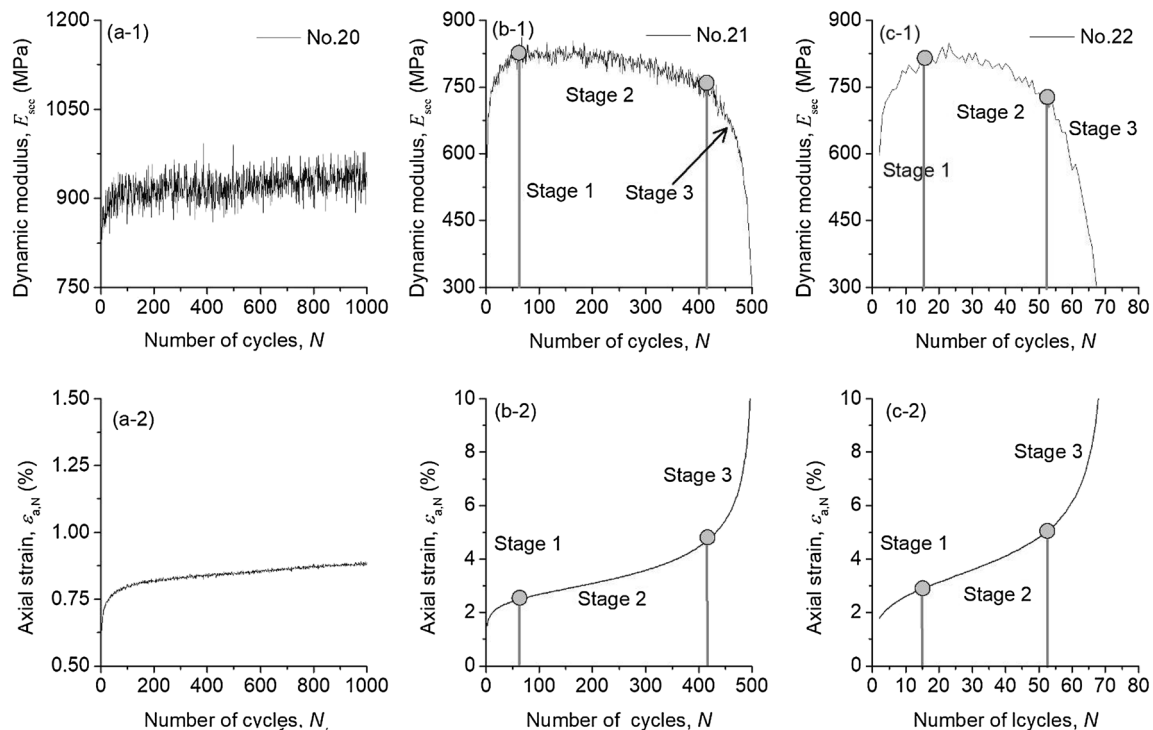


Fig. 11 Characteristics of dynamic modulus and maximum axial strain of soils under -9°C during cyclic loading **a** test No. 20 ($\sigma_d = 900$ kPa); **b** test No. 21 ($\sigma_d = 1500$ kPa); **c** test No. 22 ($\sigma_d = 1800$ kPa)

changing stiffness with increasing loading cycles, as presented in Figs. 7, 8, 9, 10 and 11. When the crack propagation grows throughout the sample and a continuous shear band is produced, the frictional resistance diminishes rapidly, which results in the accelerated increase in axial strain and rapid reduction in stiffness, as presented in stage 3 of Figs. 7, 8, 9, 10 and 11.

The changes in stiffness are often correlated with the number of loading cycles; however, the irreversible microstructures or states altered by cyclic loading are regarded as the internal reasons for these changes. Therefore, the dynamic modulus, E_{sec} , is also plotted against the axial strain, $\varepsilon_{a,N}$, in Fig. 12. It is clear that two qualitative patterns of the variation of E_{sec} with $\varepsilon_{a,N}$ are observed. For some tests (tests Nos. 13, 16 and 20), the values of E_{sec} increase with the development of $\varepsilon_{a,N}$, while E_{sec} from other tests experiences an initial nonlinear increase and then decreases with an approximate constant rate. A clear threshold yield strain, $\varepsilon_{a,yield}$, separates the change patterns of E_{sec} and the threshold yield strain, E_{sec} , reaches a peak value in these cases. From further examinations of the curves of tests Nos. 13, 16 and 20, it is clearly observed that even during the largest loading cycles, $\varepsilon_{a,N}$ is lower than that derived from the other tests. Therefore, it might be argued that no stiffness degradations are shown in these tests. This may be attributed to the lower axial strain reached relative to the threshold yield value. In addition, the threshold yield strain, $\varepsilon_{a,yield}$, and the number of loading

cycles, N_{yield} , in which the axial strain reaches the threshold values, are listed in Table 2. From this table, the values of $\varepsilon_{a,yield}$ derived from the tests under different cyclic stress levels change greatly for the samples in an unfrozen state and at a temperature of -3°C . However, the samples at -5°C , -7°C and -9°C reach their cyclic softening states at similar axial strains. The inevitable differences in samples under the same conditions may contribute to the differences in $\varepsilon_{a,yield}$. For the samples with higher ductility (the samples in an unfrozen state and at -3°C), no significant strength or stiffness loss occurs during the long deformation process and the variability of where the stress reaches the peak value is relatively large.

Unlike the static failure, the specimen failure under stress-controlled cyclic loading at a constant amplitude of cyclic stress was difficult to ascertain due to the absence of a peak stress. Thus, determining a criterion to define the cyclic failure of frozen soils under such loading conditions is a problem at the present. In the previous studies, many cyclic triaxial tests on saturated soils (clean sand, silty sand or sandy silts) under undrained conditions have been conducted mainly based on the demand for earthquake-type problems. It is often observed that the pore water pressure builds up steadily as the cyclic axial stress is applied and eventually approaches a value equal to or close (90–95%) to the initial applied confining pressure, thereby producing a sizeable amount of axial cyclic strain, which indicates that considerable softening occurs in these soils. Thus, such

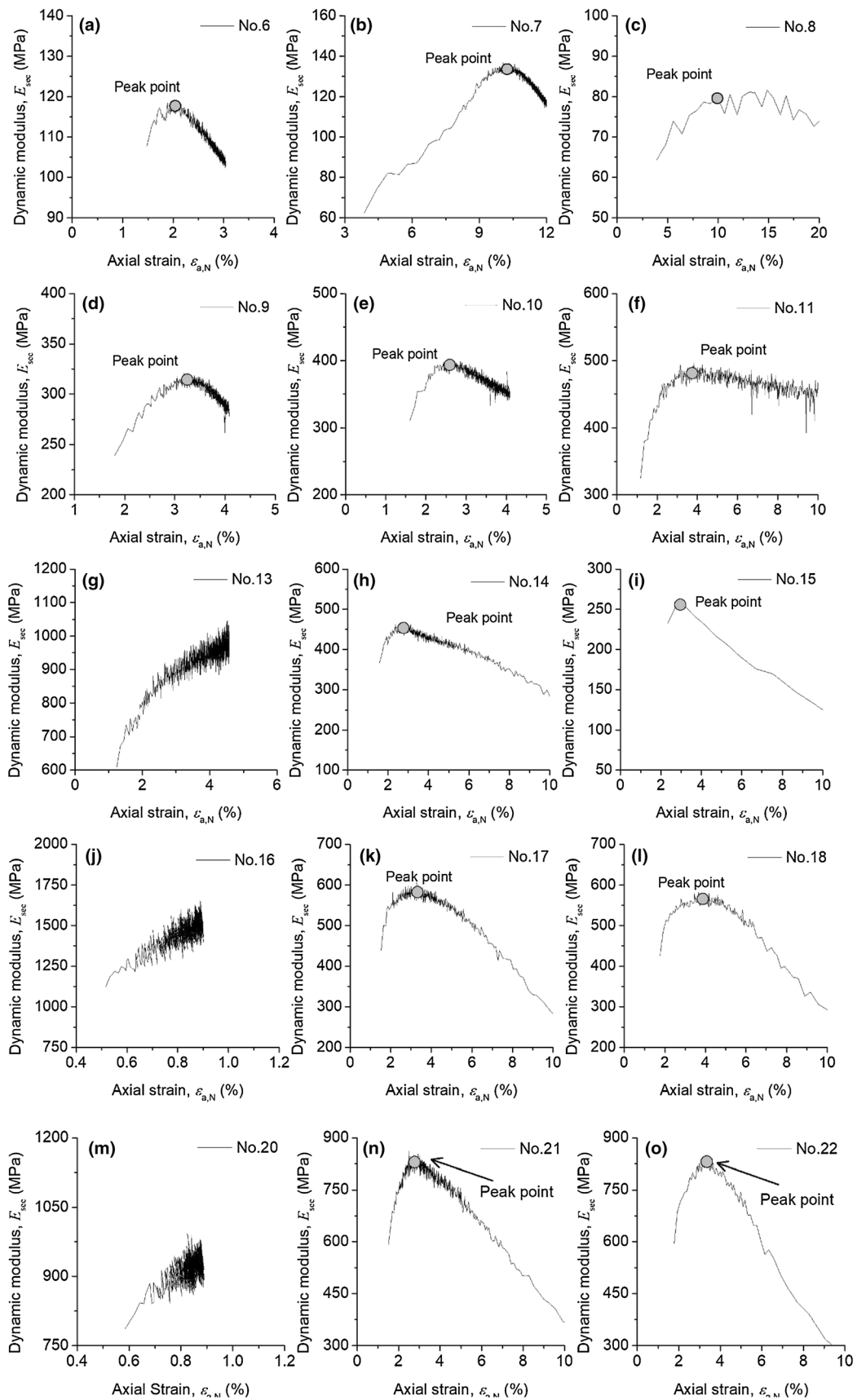


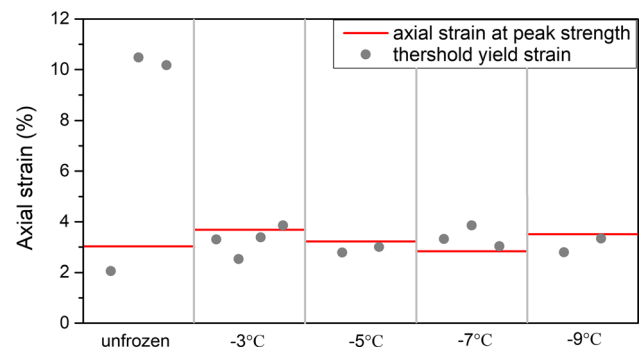
Fig. 12 Changes in dynamic modulus versus the axial strain of the tested specimens

Table 2 Summary of the threshold yield strain and yield number of loading cycles

Frozen state	Test no.	$\varepsilon_{a,yield}$ (%)	N_{yield}	Frozen state	Test no.	$\varepsilon_{a,yield}$ (%)	N_{yield}
Unfrozen	No. 6	2.06	34	− 5 °C	No. 14	2.78	56
	No. 7	10.26	119		No. 15	3.00	4
	No. 8	10.17	10	− 7 °C	No. 17	3.32	146
− 3 °C	No. 9	3.30	88		No. 18	3.85	49
	No. 10	2.52	40		No. 19	3.03	5
	No. 11	3.38	49	− 9 °C	No. 21	2.79	127
	No. 12	3.85	71		No. 22	3.34	25

a state is often utilized as a criterion to define the onset of cyclic failure or liquefaction of soils ranging from clean sands to fines containing sands [11]. However, there are some differences for frozen soils in undrained cyclic triaxial tests. First, the undrained condition is usually nominal for frozen soils and no liquid water flow out of the test samples is detected in most cases. Second, so far, no effective device can measure the pore stress in frozen soils, and hence, the pore stress cannot be used as an index to evaluate the strength state of frozen soils. Third, residual deformation is the major pattern of frozen soils under such one-way cyclic loading without stress reversal, and no significant level of cyclic strain can be reached even after a very large number of loading cycles. Turning attention back to the plot in Fig. 12, the dynamic modulus, E_{sec} , will degrade after the threshold yield strain, $\varepsilon_{a,yield}$, which means the cyclic softening takes places at that moment. Compared with the liquefaction state of saturated soils in the unfrozen state in the previous studies, the strength and stiffness of frozen soils do not dissipate completely in this state, which appears to be more similar to the peak strength derived from the monotonic triaxial tests. Therefore, the state where E_{sec} begins to degrade may be an option to define the criterion of cyclic failure.

To further evaluate the soundness of this criterion, the threshold yield strain derived from cyclic triaxial tests and the yield strain at peak strength derived from monotonic triaxial tests are plotted in Fig. 13. It is clearly observed that there is considerable scatter in the data derived from the tests with soils in the unfrozen state, while the threshold yield strains derived from cyclic tests are near the yield strain for the frozen soils, especially at low temperatures (− 5 °C, − 7 °C and − 9 °C). The observations presented here are consistent with the behavior exhibited in the stress–strain curves in Fig. 3. For the samples with high ductility, the stress often changes smoothly after a threshold axial strain, and the variability of where the stress reaches the peak value is relatively large. Thus, the criterion of cyclic failure presented above is more suitable for frozen soils at low temperatures. Furthermore, the plot also

**Fig. 13** The threshold yield strain derived from cyclic triaxial tests and the yield strain at peak strength derived from monotonic triaxial tests

suggests that the deformation pattern of frozen samples with high brittleness is consistent under both monotonic as well as cyclic loading, and the criterion of cyclic failure is consistent with the peak strength derived from the monotonic triaxial test.

Following the routine practice of cyclic resistance of saturated soils in an unfrozen state [11], the cyclic stress ratio is defined as $\sigma_d/(2\sigma_3)$ for the triaxial loading condition of frozen soils, which considers the combined effect of cyclic shear stress and confining pressure. In Fig. 14, the cyclic stress ratio is plotted versus the number of cycles required to produce cyclic failure. It can be observed that a large cyclic stress ratio does not correspond to a small number of cycles, as expected for the samples in an unfrozen state and at − 3 °C, which also means that the criterion of cyclic failure presented above is not reasonable for the soils with high ductility. Therefore, it is better to define it at an arbitrary level of axial strain. Compared with the data derived from the tests at − 5 °C, − 7 °C and − 9 °C, the samples at lower temperatures correspond to a higher cyclic stress ratio given the same number of loading cycles. Although there are few data points, the tendency of the effect is clear, which is consistent with the conclusion derived from the monotonic tests.

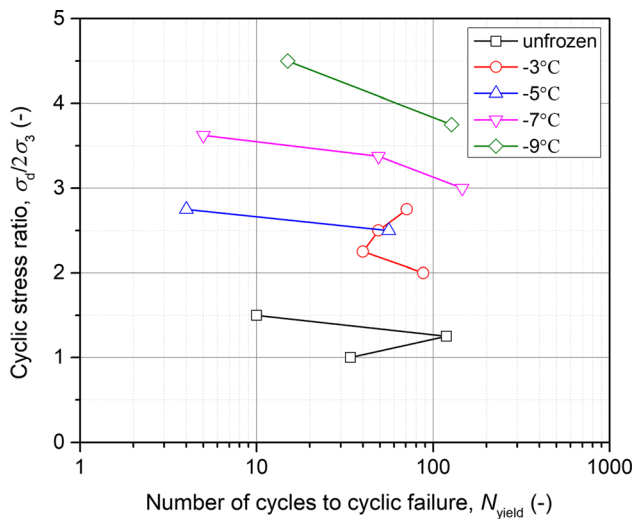


Fig. 14 Results of the cyclic strength of the specimens under unfrozen state and different temperatures

4 Summary and conclusions

A series of monotonic and cyclic triaxial tests was conducted on artificial soil samples in an unfrozen state and at different temperatures. Their strength and stiffness behaviors were investigated in detail, and several important findings were made and are summarized below.

- (1) The patterns of stress–strain curves of test specimens under monotonic loading change with decreasing frozen temperature. The samples tested at lower temperature were found to have higher brittleness, and the peak strength and stiffness increase with decreasing temperature. These changes are mainly attributed to the stronger cementation between the solid particles at lower frozen temperature. Furthermore, the effect of temperature on the peak strength and stiffness can be described well by one and the same linear equation.
- (2) In the cyclic loading sequence, the stress–strain curve of soils tested shows hysteresis and accumulation of irreversible strains with increasing number of cycles. For the tests under high-level cyclic loading (reaching the test limit in fewer than 1000 cycles), the evolution of the axial strain and dynamic modulus shows different development patterns for soils in different frozen states. The test samples in an unfrozen state and at $-3\text{ }^{\circ}\text{C}$ exhibit two deformation stages: (i) In the initial stage, both the axial strain and stiffness increase with increasing loading cycles, and (ii) in the subsequent stage, the axial strain increases with a near constant rate, while the dynamic modulus remains constant or decreases smoothly. However, the deformation process of test

soils at $-5\text{ }^{\circ}\text{C}$, $-7\text{ }^{\circ}\text{C}$ and $-9\text{ }^{\circ}\text{C}$ includes three stages, and accelerated increases in axial strain and rapid reductions in stiffness are observed in the last stage.

- (3) Two mechanisms, namely volumetric compaction and frictional sliding, are employed to explain the deformation process of soils under triaxial compression conditions. The different deformation patterns of test samples in different frozen states are primarily induced in the process of frictional sliding. The frictional sliding process of specimens with high brittleness is similar to the fracturing of solid materials, and when crack propagation grows throughout the sample and a continuous shear band is produced, the frictional resistance will dissipate rapidly, which results in accelerated increases in axial strain and rapid reductions in stiffness.
- (4) The evolution of stiffness with the development of axial deformation comprises an initial nonlinearly increasing stage and an approximately linearly decreasing stage. In addition, a peak value of the dynamic modulus can be derived from the evolution curve and the state where the cyclic softening occurs is proposed as the criterion of cyclic failure of soils under cyclic triaxial compression conditions.
- (5) This criterion was further examined by comparing the threshold axial strain under cyclic loading and yield axial strain at peak strength in monotonic loading. It is observed that their variability is small for the samples at $-5\text{ }^{\circ}\text{C}$, $-7\text{ }^{\circ}\text{C}$ and $-9\text{ }^{\circ}\text{C}$, which indicates that the criterion of cyclic failure proposed in this study shows good performance for frozen soils with high brittleness. Following the routine practice of soil dynamics, the cyclic stress ratios are plotted versus the number of loading cycles to the proposed cyclic failure, and a clear observation that the samples at lower temperature had a higher cyclic strength was found.

Acknowledgements The authors appreciate the valuable comments from the anonymous reviewers which made the submitted paper very much improved. The authors also gratefully acknowledge the financial support of (1) the National Nature Science Foundation of China (Grant Nos. 51708522, 51769018, 51879131, 41627801 and 11702304), (2) the Heilongjiang Provincial Nature Science Foundation of China (Grant No. E2018059) and (3) the project supported by science and technology department of Jiangxi province of China (Grant No. 20161BBG70084).

References

1. Al-Hunaidi M, Chen P, Rainer J, Tremblay M (1996) Shear moduli and damping in frozen and unfrozen clay by resonant column tests. *Can Geotech J* 33(3):510–514

2. Andersen GR, Swan CW, Ladd CC, Germaine JT (1995) Small-strain behavior of frozen sand in triaxial compression. *Can Geotech J* 32(3):428–451
3. Arenson LU, Springman SM (2005) Mathematical descriptions for the behaviour of ice-rich frozen soils at temperatures close to 0 C. *Can Geotech J* 42(2):431–442
4. Arenson LU, Springman SM (2005) Triaxial constant stress and constant strain rate tests on ice-rich permafrost samples. *Can Geotech J* 42(2):412–430
5. Chamberlain E, Groves C, Perham R (1972) The mechanical behaviour of frozen earth materials under high pressure triaxial test conditions. *Geotechnique* 22:469–483
6. Cheng G (2005) A roadbed cooling approach for the construction of Qinghai-Tibet Railway. *Cold Reg Sci Technol* 42(2):169–176
7. Czurda KA, Hohmann M (1997) Freezing effect on shear strength of clayey soils. *Appl Clay Sci* 12(1–2):165–187
8. Da Re G, Germaine JT, Ladd CC (2003) Triaxial testing of frozen sand: equipment and example results. *J Cold Reg Eng* 17(3):90–118
9. Hu X, Fang T (2014) Numerical simulation of temperature field at the active freeze period in tunnel construction using freeze-sealing pipe roof method. In: Ding W, Li X (eds) *Geo-Shanghai 2014: tunnel and underground construction*, ASCE, Shanghai, pp 731–741
10. Hu X, Deng S, Ren H (2016) In situ test study on freezing scheme of freeze-sealing pipe roof applied to the gongbei tunnel in the Hong Kong-Zhuhai-Macau bridge. *Appl Sci* 7(1):27
11. Ishihara K (1996) *Soil behaviour in earthquake geotechnics*. Oxford Science Publications, Oxford, pp 219–221
12. Kornfeld T, Zubeck H (2013) Triaxial testing of frozen soils-state of the art. In: Zubeck H, Yang Z (eds) *Selected technical papers STP1568: mechanical properties of frozen soils*. ASTM International, pp 76–85
13. Lackner R, Amon A, Lagger H (2005) Artificial ground freezing of fully saturated soil: thermal problem. *J Eng Mech* 131(2):211–220
14. Lai Y, Xu X, Dong Y, Li S (2013) Present situation and prospect of mechanical research on frozen soils in china. *Cold Reg Sci Technol* 87(87):6–18
15. Lai Y, Xu X, Yu W, Qi J (2014) An experimental investigation of the mechanical behavior and a hyperplastic constitutive model of frozen loess. *Int J Eng Sci* 84:29–53
16. Li JC, Baladi GY, Andersland OB (1979) Cyclic triaxial tests on frozen sand. *Eng Geol* 13(1–4):233–246
17. Li Q, Ling X, Hu J, Zhou Z (2019) Residual deformation and stiffness changes of frozen soils subjected to high-and low-amplitude cyclic loading. *Can Geotech J* 56(2):263–274
18. Liu E, Lai Y, Liao M, Liu X, Hou F (2016) Fatigue and damage properties of frozen silty sand samples subjected to cyclic triaxial test. *Can Geotech J* 53:1939–1951
19. Ling X, Li Q, Wang L, Zhang F, An L, Xu P (2013) Stiffness and damping ratio evolution of frozen clays under long-term low-level repeated cyclic loading: experimental evidence and evolution model. *Cold Reg Sci Technol* 86:45–54
20. Ma W, Wu Z, Zhang L, Chang X (1999) Analyses of process on the strength decrease in frozen soils under high confining pressures. *Cold Reg Sci Technol* 29:1–7
21. Ma W, Cheng G, Wu Q (2009) Construction on permafrost foundations: lessons learned from the Qinghai-Tibet railroad. *Cold Reg Sci Technol* 59(1):3–11
22. Ma L, Qi J, Fan Y, Yao X (2016) Experimental study on variability in mechanical properties of a frozen sand as determined in triaxial compression tests. *Acta Geotech* 11(1):61–70
23. Parameswaran VR (1980) Deformation behaviour and strength of frozen sand. *Can Geotech J* 17(1):74–88
24. Qi J, Ma W (2007) A new criterion for strength of frozen sand under quick triaxial compression considering effect of confining pressure. *Acta Geotech* 2(3):221
25. Sheng D, Zhang S, Niu F, Cheng G (2014) A potential new frost heave mechanism in high-speed railway embankments. *Geotechnique* 64:144–154
26. Vaziri H, Han Y (1991) Full-scale field studies of the dynamic response of piles embedded in partially frozen soils. *Can Geotech J* 28(5):708–718
27. Vinson TS, Chaichanavong T, Li JC (1978) *Dynamic testing of frozen soils under simulated earthquake loading conditions*. ASTM Special Technical Publication, West Conshohocken, pp 65–71
28. Wang DY, Ma W, Wen Z, Chang XX (2008) Study on strength of artificially frozen soils in deep alluvium. *Tunn Undergr Sp Technol* 23(4):381–388
29. Wang J, Nishimura S, Okajima S, Joshi BR (2018) Small-strain deformation characteristics of frozen clay from static testing. *Géotechnique* 1–12
30. Wood DM (1990) *Soil behaviour and critical state soil mechanics*. Cambridge University Press, Cambridge
31. Wheeler SJ, Sivakumar V (1995) An elasto-plastic critical state framework for unsaturated soil. *Géotechnique* 45(1):35–53
32. Yuko Yamamoto, Springmansarah M (2014) Axial compression stress path tests on artificial frozen soil samples. *Can Geotech J* 51(10):1178–1195
33. Yang P, Ke JM, Wang JG, Chow YK, Zhu FB (2006) Numerical simulation of frost heave with coupled water freezing, temperature and stress fields in tunnel excavation. *Comput Geotech* 33(6):330–340
34. Zhang D, Li Q, Liu E, Liu X, Zhang G, Song B (2019) Dynamic properties of frozen silty soils with different coarse-grained contents subjected to cyclic triaxial loading. *Cold Reg Sci Technol* 157:64–85
35. Zhang G, Liu E, Chen S, Zhang D, Liu X, Yin X, Song B (2018) Effects of uniaxial and triaxial compression tests on the mechanical properties of frozen sandstone samples using real-time CT scanning technique. *Int J Phys Model Geotech*. <https://doi.org/10.1680/jphmg.18.00006>
36. Zhang S, Tang CA, Zhang XD, Zhang ZC, Jin JX (2015) Cumulative plastic strain of frozen aeolian soil under highway dynamic loading. *Cold Reg Sci Technol* 120:89–95
37. Zhou Z, Ma W, Zhang S, Du H, Mu Y, Li G (2016) Multiaxial creep of frozen loess. *Mech Mater* 95:172–191
38. Zhou Z, Ma W, Zhang S, Mu Y, Li G (2018) Effect of freeze-thaw cycles in mechanical behaviors of frozen loess. *Cold Reg Sci Technol* 146:9–18
39. Zhou Z, Ma W, Zhang S, Du H, Mu Y, Li G (2018) Damage evolution and recrystallization enhancement of frozen loess. *Int J Damage Mech* 27(8):1131–1155

Publisher's Note Springer Nature remains neutral with regard to jurisdictional claims in published maps and institutional affiliations.